

Joint optimization of *fitting & matching* in multi-view reconstruction

Hossam Isack Yuri Boykov

Computer Science Department

Western University, Canada

habdelka@csd.uwo.ca, yuri@csd.uwo.ca

Feb. 21, 2013

Abstract

Many standard approaches to geometric model fitting are based on pre-matched image features. Typically, such pre-matching uses only feature appearances (e.g. SIFT) and a large number of non-unique features must be discarded in order to control the false positive rate. In contrast, we solve feature matching and multi-model fitting problems in a joint optimization framework. This paper proposes several *fit- \mathcal{E} -match* energy formulations based on a generalization of the *assignment problem*. To find near optimal solutions, we developed an efficient solver based on *min-cost-max-flow* algorithm. Our approach significantly increases the number of detected matches. In practice, energy-based joint *fitting & matching* allows to increase the distance between view-points previously restricted by robustness of local SIFT-matching and to improve the model fitting accuracy when compared to the state-of-the-art.

1 Introduction

Many existing methods for model fitting and 3D structure estimation use prematched image features as an input (bundle adjustment [1], homography fitting [2, 3], rigid motion estimation [4, 5, 6]). Vice versa, many matching methods (sparse/dense stereo) often use some preestimated structural constraints, e.g. epipolar geometry, to identify correct matches/inliers. This paper introduces a novel framework for simultaneous estimation of high-level structures (multi-model fitting) and low-level correspondences (feature matching). We discuss several regularization-based formulations

of the proposed *fit & match* (FM) problem. These formulations use a generalization of the *assignment problem* and we use efficient specialized *min-cost-max-flow* solver that has been overlooked in the computer vision community. This paper primarily focuses on jointly solving multi-homography fitting and sparse feature matching as a simple show case for the FM paradigm. Other applications would be rigid motions estimation, camera pose estimation [7], etc.

Related Work: In case of reliable matching, RANSAC is a well-known robust method for single model fitting. The main idea is to generate a number of model proposals by randomly sampling the matches and then select one model with the largest set of inliers (a.k.a. consensus set) with respect to some fixed threshold. In case of unreliable matching, e.g. repetitive texture or wide view-point, RANSAC or any technique that relies on pre-computed matching would fail.

Guided-MLESAC [8] and PROSAC [9] are RANSAC generalizations that try to overcome unreliable matches while generating model hypotheses. Their main idea is to ensure that matches with high matching scores are more likely to get sampled, thus “guiding” the sampling process while generating model hypotheses. One could argue that these techniques would still fail since false matches could also have high matching scores, e.g. scenes with repetitive texture. SCRAMSAC [10] is a form of spatial guided sampling that uses a spatial consistency filter to restrict the sampling domain to matches with similar local geometric consistency. This method is sensitive to the ratio of occluded/unoccluded features, as in that case the assumption that correct matches form a dense cluster is no longer valid. The main drawback of these RANSAC generalizations is that they focus on generating a reliable model hypotheses by using pre-matched features (fixed matching). That drawback could be avoided by jointly solving the matching and fitting problems.

An attempt to formulate an objective function for *fitting-&-matching* naturally leads to a version of the assignment problem. The majority of prior work could be divided into two major groups: matching techniques using quadratic assignment problems and FM techniques using linear assignment subproblems.

Quadratic assignment problem (QAP) normally appears in the context of non-parametric matching. For example, the methods in [11, 12, 13] estimate non-rigid motion correspondences as a sparse vector field. They rely on a quadratic term in the objective function to encourage geometric regularity between identified matched pairs. Such QAP formulations often appear in shape matching and object recognition. QAP is NP-hard and these methods use different techniques to approximate it. For example, [14] approximates QAP by iteratively minimizing its first-order Taylor expansion, which reduces to a *linear assignment problem* (LAP).

If correspondences are constrained by some parametric model(s), matching often simplifies to LAP when model parameters are fixed. In this case, the geometric regularity is enforced by a model fidelity term (linear w.r.t. matching variables) and pair-wise consistencies [11, 12, 13] are no longer needed. Typically for FM problems, LAP-based feature matching and model parameter fitting are preformed in a *block coordinate descent* (BCD) fashion. For example, SoftPOSIT [7] matches 2D image features to 3D object points and estimate camera pose in such iterative fashion. Building on the ideas in SoftPOSIT Serradell et al. [15] fit a single homography using geometric and appearance priors with unknown correspondences. It should be noted that although SoftPOSIT solves for the matching by using *softassign* [14]—which will result in an approximate matching. SoftPOSIT justified using *softassign* by claiming that the objective function is non-linear. That claim is not exactly accurate as SoftPOSIT uses BCD to minimize that non-linear objective function. Thus, when solving for the matching all the other parameters are fixed and the objective function becomes linear in terms of the matching variables. For linear objective function the optimal matching could be found by using a Linear Programming solver¹.

Our work develops a generalization of LAP for solving FM problem when matching is constrained by an unknown number of geometric models. In contrast to [7, 15], we do not assume that matches/correspondences are constrained by a single parametric model. Note that in order to solve FM problem for multi-models, a regularization term is required to avoid over fitting. Unlike [15, 7], our energy formulation includes label cost regularization [16] and spatial regularization as in some QAP approaches to matching [11].

Contribution: In this work we propose two FM energy functionals (3) and (5) for jointly solving matching and multi-model fitting. Energy (3) consists of two terms: unary potentials for matching similar features and assigning matched features to their best fitting geometric models, and a label cost term to discourage overfitting by penalizing the number of labels/models assigned to matches. Energy (5) consists of unary potential and label cost terms, as in energy (3), and a pairwise potential term for encouraging nearby matches to be assigned to the same label/model.

The key subproblem when minimizing (3) or (5) in BCD fashion is *generalized assignment problem* (GAP), which is our novel generalization of LAP to mutli-model case. GAP jointly formulates feature-to-feature matching and match-to-model assignment. We propose a fast globally optimal approach for GAP by generalizing *min-cost-max-flow* techniques for single model LAP matching [17].

¹SoftPOST use of *softassign* to find the matching could be attributed to performance gains, as LP solvers will be considerably slow for large problems.

Figure 8 compares the results of a standard energy-based multi-model fitting algorithm [16] (EF) and our proposed energy-based multi-model *fitting- \mathcal{E} -matching* algorithm (EFM). EF used the standard pre-matching technique in [18] that rejected a relatively large number of true matches. EFM found better models' estimates because it nearly doubled the number of identified matches.

2 Our Approach

Standard techniques for sparse feature matching [18] independently decide each match relying on the discriminative power of the used feature descriptor. These techniques are prone to ignoring a large number of non-distinct image features that could have been valid matches. Our unified framework simultaneously estimate high-level structures (multi-model fitting) and low-level correspondences (features matching). Unlike standard techniques, our approach is less vulnerable to the descriptor's discriminative power. We discuss regularization-based formulation of the proposed *fit \mathcal{E} match* problem. While there are many different applications for a general FM paradigm, this work primarily focuses on jointly solving geometric multi-model fitting (homographies) and sparse feature matching.

We will use the following notations in defining our energy:

| | | |
|-----------------|----|---|
| \mathcal{F}_l | - | set of all observed features in the left image. |
| \mathcal{F}_r | - | set of all observed features in the right image. |
| \mathcal{L} | - | a set of randomly sampled homographies (labels). |
| f_p | - | label assigned to feature p such that $f_p \in \mathcal{L}$ |
| f | - | a <i>labeling</i> of all features in the left image, $f = \{f_p p \in \mathcal{F}_l\}$ |
| θ_h | - | parameters of homography h from left image to right image. |
| θ | - | set of all models' (homographies) parameters. |
| S_l | - | Subset of features in the left image supporting one geometric model (plane, homography), see Figs (4)(a-b). |
| S_r | - | Subset of features in the right image supporting one geometric model (plane, homography), see Figs (4)(a-b). |
| x_{pq} | - | is a binary variable which is 1 if p and q are matched (assigned) to each other and 0 otherwise. |
| \mathcal{M} | := | $\{x_{pq} (p, q) \in \mathcal{F}_l \times \mathcal{F}_r\}$. |
| $Q(p, q)$ | - | appearance penalty for features $p \in \mathcal{F}_l$ and $q \in \mathcal{F}_r$ based on similarity of their descriptors. |
| \mathcal{N} | - | edges of near-neighbor graph, e.g. delaunay triangulation, for left image features. |

2.1 Energy

We will define the overall matching score between two features $p \in \mathcal{F}_l$ and $q \in \mathcal{F}_r$ as a function of geometric transformation θ_h

$$D_{pq}(\theta_h) = \|\theta_h \cdot p - q\| + Q(p, q) \quad (1)$$

combining the geometric error and the appearance penalty where $\|\cdot\|$ denotes geometric transfer error. A similar matching score was used in computing the ground truth matching in [19, 20]. We can also use a symmetric matching score

$$D_{pq}(\theta_h) = \|\theta_h \cdot p - q\| + \|\theta_h^{-1} \cdot q - p\| + Q(p, q). \quad (2)$$

We are only interested in symmetric appearance penalty $Q(p, q)$, e.g. the angle (or some metric distance) between the features' descriptors of p and q . From here on D_{pq} refers to the symmetric matching score.

In this work, $Q(p, q) = 0$ if the angle between the two features' descriptors is less than $\pi/4$ and ∞ otherwise. The aforementioned non-continuous appearance penalty is less sensitive to the descriptor's discriminative power in comparison to the continuous one.

To simplify our formulation we will introduce our energies under the assumption that there are no occlusions

$$E_1(f, \theta, \mathcal{M}) = \sum_{\substack{p \in \mathcal{F}_l \\ q \in \mathcal{F}_r}} D_{pq}(\theta_{f_p}) \cdot x_{pq} + \beta \sum_{h \in \mathcal{L}} \delta_h(f) \quad (3)$$

$$\text{s.t.} \quad \left. \begin{array}{l} \sum_{p \in \mathcal{F}_l} x_{pq} = 1 \quad \forall q \in \mathcal{F}_r \\ \sum_{q \in \mathcal{F}_r} x_{pq} = 1 \quad \forall p \in \mathcal{F}_l \\ x_{pq} \in \{0, 1\} \quad \forall p \in \mathcal{F}_l, \forall q \in \mathcal{F}_r \end{array} \right\} \quad (4)$$

where $\delta_h(f) = [\exists p \in \mathcal{F}_l : f_p = h]$ and $[\cdot]$ are *Iverson brackets*, and

$$E_2(f, \theta, \mathcal{M}) = \sum_{\substack{p \in \mathcal{F}_l \\ q \in \mathcal{F}_r}} D_{pq}(\theta_{f_p}) \cdot x_{pq} + \lambda \sum_{(p,q) \in \mathcal{N}} [f_p \neq f_q] + \beta \sum_{h \in \mathcal{L}} \delta_h(f) \quad (5)$$

under constraints (4). We will show how to handel outliers/occlusions in Section 3.1. E_2 is more powerful than E_1 because the spatial regularizer eliminates the artifacts that results from using only one regularizer in E_1 . The reader is referred to [16] for a more detailed discussion comparing E_1 and E_2 for fixed matching in the context of multi-model fitting.

2.2 Optimization

In this section, we describe an efficient approach, EFM₁, to minimize E_1 in a *block coordinate decent* (BSD) fashion, and a second approach, EFM₂, to minimize E_2 .

Energy-based Fitting & Matching for E_1 (EFM₁)

Initialization: Find an initial \mathcal{M} using standard matching techniques

repeat

 Given \mathcal{M} , solve (6) using PEARL [16] for f and θ

 Given θ , solve (7)-(8) using LS-GAP, see Sec. 3.2, for \mathcal{M} and f

until E_1 converges

EFM₁ finds an initial matching using standard matching techniques and then it iteratively minimizes E_1 by alternating between solving for f and θ while fixing \mathcal{M} , and solving for f and \mathcal{M} while fixing θ . Although EFM₁ is guaranteed to converge since E_1 is bounded below, i.e. $E_1 \geq \beta$, it is not trivial to derive a theoretical bound on the convergence rate and approximation ratio of EFM₁. However, in Section 5, we empirically show that EFM₁ converges in a few iterations to a near optimal solution.

On the one hand, E_1 for fixed \mathcal{M} reduces to

$$E(f, \theta) = \sum_{p \in \mathcal{F}_l} D_p(\theta_{f_p}) + \beta \sum_{h \in \mathcal{L}} \delta_h(f) \quad (6)$$

where $D_p(\theta_h) = D_{pq}(\theta_h) \ \forall h \in \mathcal{L}$ provided that q is assigned to p by \mathcal{M} , i.e. $x_{pq} = 1$. Furthermore, energy (6) could be efficiently solved for f, θ using PEARL [16].

On the other hand, E_1 for fixed θ could be re-parameterized and written in the following form

$$\begin{aligned} E(\mathcal{M}_f) &= \sum_{h \in \mathcal{L}} \sum_{p \in \mathcal{F}_l} \sum_{q \in \mathcal{F}_r} D_{pq}(\theta_h) x_{pqh} + \beta \sum_{h \in \mathcal{L}} \delta_h(\mathcal{M}_f) & (7) \\ \text{s.t.} & \left. \begin{aligned} \sum_{h \in \mathcal{L}} \sum_{p \in \mathcal{F}_l} x_{pqh} &= 1 \quad \forall q \in \mathcal{F}_r \\ \sum_{h \in \mathcal{L}} \sum_{q \in \mathcal{F}_r} x_{pqh} &= 1 \quad \forall p \in \mathcal{F}_l \\ x_{pqh} &\in \{0, 1\} \quad \forall h \in \mathcal{L}, p \in \mathcal{F}_l, q \in \mathcal{F}_r \end{aligned} \right\} & (8) \end{aligned}$$

where binary variable x_{pqh} is 1 if p and q are matched to each other and assigned to model h , and 0 otherwise. Matching \mathcal{M}_f is defined as $\{x_{pqh} \mid (p, q, h) \in \mathcal{F}_l \times \mathcal{F}_r \times \mathcal{L}\}$ encapsulating information of both feature-to-feature and match-to-model assignments, and δ_h is now defined as $\delta_h(\mathcal{M}_f) = [\exists p \in \mathcal{F}_l, q \in \mathcal{F}_r : x_{pqh} = 1]$. We

will refer to the special unregularized case of optimization problem (7)-(8) where $\beta = 0$ as the *generalized assignment problem* (GAP) ².

This is a weighted matching problem over a fixed set of multiple models that match features and assigns each match to a model. GAP is an *integral linear program*, see Appendix B for proof, and therefore any Linear Programming toolbox could be used to find its optimal solution by solving its relaxed LP—but will be considerably slow due to the size of the problem at hand, as shown in Section 3.2. A fast approach to solve GAP is described in Section 3.1. The optimal solution for GAP may overfit models to data since the number of models is not regularized when $\beta = 0$. For $\beta > 0$ optimization problem (7)-(8) could be solved using LS-GAP, introduced in Section 3.2, which utilizes a fast GAP solver in a combinatorial local search algorithm. This local search over different subsets of \mathcal{L} selects a solution reducing energy (7).

Energy-based Fitting & Matching for E_2 (EFM₂)

Initialization: Find an initial \mathcal{M}, f, θ using EFM₁

repeat

 Given \mathcal{M} , solve (9) using PEARL for f and θ

 Given f, θ , solve (10)-(4) using LC-GAP, see Sec. 3.3, for \mathcal{M}

until E_2 converges

EFM₂ uses EFM₁ result as an initial solution and then iteratively minimizes E_2 by alternating steps solving for f and θ while fixing \mathcal{M} , and solving for \mathcal{M} while fixing θ and f . Energy (5) for fixed \mathcal{M} reduces to

$$E(f, \theta) = \sum_{p \in \mathcal{F}_l} D_p(\theta_{f_p}) + \lambda \sum_{(p,q) \in \mathcal{N}} [f_p \neq f_q] + \beta \sum_{h \in \mathcal{L}} \delta_h(f) \quad (9)$$

and is solved using PEARL. For fixed f and θ energy (5) reduces to

$$E(\mathcal{M}) = \sum_{p \in \mathcal{F}_l} \sum_{q \in \mathcal{F}_r} D_{pq}(\theta_{f_p}) x_{pq} \quad (10)$$

under constraints (4). Energy (10) is solved using label constrained GAP (LC-GAP), Section 3.3. LC-GAP is a variant of the fast GAP solver that can change feature-to-feature matching without affecting the current labeling. It should be noted that, based on our experience, EFM₂ slightly modifies the initial solution by rejecting or correctly matching less than a handful of false positives. Therefore, in practice we suggest to run only one iteration of EFM₂ to reject the false positives incorrectly matched due to lack of spatial coherency.

²Our definition of GAP is different from the formal definition in optimization literature.

3 Algorithms

We introduce a fast GAP solver, in Section 3.1, to minimize energy (7)-(8) for $\beta = 0$. Section 3.2 covers LS-GAP algorithm which is used in EFM₁ to minimize energy (7)-(8) for $\beta > 0$. Finally, in Section 3.3, we describe LC-GAP which is used in EFM₂ to minimize energy (10).

3.1 A fast GAP solver

As stated earlier, GAP is an *integral linear program* and therefore any LP solver could be used to find its optimal solution. However, LP solvers will be slow considering large number of decision variables for GAP instances in our application. In this section, we show that our GAP problem (equations (7)-(8) for $\beta = 0$) can be equivalently reformulated as a standard *min-cost-max-flow* (MCMF) problem for which very efficient specialized solvers are known. In the case of a single model, it is well-known that an assignment problem (AP) can be solved by finding MCMF on a particular graph [17]. One of our contributions is a more general graph construction for formulating multi-model assignment problem, i.e. GAP, as an instance of MCMF.

We will first state the formal definition of MCMF before introducing our formulation. Let $\mathcal{G} = (\mathcal{V}, \mathcal{E})$ denote a graph with vertices \mathcal{V} such that $s, t \in \mathcal{V}$, and edges \mathcal{E} where each edge $(v, w) \in \mathcal{E}$ has a capacity $u(v, w)$ and cost $c(v, w)$. The cost of on an arbitrary valid flow function \mathbf{F} is defined as

$$\text{cost}(\mathbf{F}) = \sum_{(v,w) \in \mathcal{E}} c(v, w) \cdot \mathbf{F}(v, w).$$

A flow that maximizes the amount of flow passed from s to t while minimizing the cost is the MCMF.

To formulate GAP as MCMF problem we build graph $\mathcal{G}^* = (\mathcal{V}, \mathcal{E})$, see Fig. 1(a), with the set of nodes

$$\begin{aligned} \mathcal{V} = & \{s, t\} \cup \{n_p \mid p \in \mathcal{F}_l\} \cup \{n_q \mid q \in \mathcal{F}_r\} \cup \\ & \{n_{ph} \mid p \in \mathcal{F}_l, h \in \mathcal{L}\} \cup \{n_{qh} \mid q \in \mathcal{F}_r, h \in \mathcal{L}\}, \end{aligned}$$

the set of edges

$$\begin{aligned} \mathcal{E} = & \{(s, n_p) \mid p \in \mathcal{F}_l\} \cup \\ & \{(n_p, n_{ph}) \mid p \in \mathcal{F}_l, h \in \mathcal{L}\} \cup \\ & \{(n_{ph}, n_{qh}) \mid p \in \mathcal{F}_l, q \in \mathcal{F}_r, h \in \mathcal{L}\} \cup \\ & \{(n_{qh}, n_q) \mid q \in \mathcal{F}_r, h \in \mathcal{L}\} \cup \\ & \{(n_q, t) \mid q \in \mathcal{F}_r\}, \end{aligned}$$

and the following edge capacity u and edge cost c functions

$$u(v, w) = 1 \quad \text{for } (v, w) \in \mathcal{E}$$

$$c(v, w) = \begin{cases} D_{pq}(\theta_h) & \text{for } (v, w) \in \{(n_{ph}, n_{qh}) \mid p \in \mathcal{F}_l, q \in \mathcal{F}_r, h \in \mathcal{L}\} \\ 0 & \text{otherwise.} \end{cases}$$

Lemma 3.1 *The optimal solution for a feasible GAP (eq. (7)-(8) for $\beta=0$) is*

$$\mathcal{M}_f = \{x_{pqh} = \mathbf{F}^*(n_{ph}, n_{qh}) \mid p \in \mathcal{F}_l, q \in \mathcal{F}_r, h \in \mathcal{L}\}$$

where $\mathbf{F}^* : \mathcal{E} \rightarrow \{0, 1\}$ is the MCMF over graph \mathcal{G}^* .

Using Lemma 3.1, see proof Appendix A, a GAP solution \mathcal{M}_f could be found by using an efficient MCMF algorithm [17].

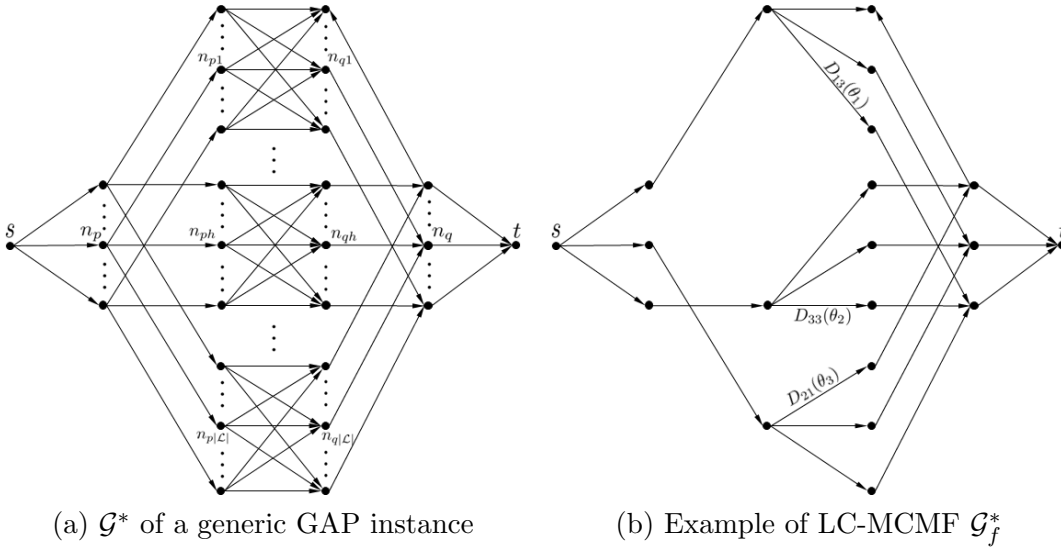


Figure 1: Figure (a) shows the generalized graph construction \mathcal{G}^* of a generic GAP instance—with unit capacity edges and edge cost function $c(v, w) = D_{pq}(\theta_h)$ for all $(v, w) \in \{(n_{ph}, n_{qh}) \mid \forall p \in \mathcal{F}_l, q \in \mathcal{F}_r, h \in \mathcal{L}\}$ and 0 otherwise. This construction does not assume that $|\mathcal{F}_l| = |\mathcal{F}_r|$. Figure (b) shows \mathcal{G}_f^* of a GAP with $|\mathcal{F}_l| = |\mathcal{F}_r| = 3$ and $|\mathcal{L}| = 3$ under the labeling constraint $f = [1 \ 3 \ 2]$.

Occlusions/Outliers: GAP might be unfeasible due to occlusions and in that case $|\mathcal{F}_l| \neq |\mathcal{F}_r|$. We add $||\mathcal{F}_l| - |\mathcal{F}_r||$ dummy features, with a fixed matching cost T , to the smaller set of features to ensure GAP feasibility. This is equivalent to changing a rectangular assignment problem to a square one. Also, to make our approach is robust to outliers we introduce an outlier model ϕ such that $D_{pq}(\phi) = T$ for any $p \in \mathcal{F}_l$ and $q \in \mathcal{F}_r$. The use of an outlier model with a uniformly distributed cost is a common technique in Computer Vision [16, 21].

3.2 Local Search-GAP (LS-GAP)

Now we introduce a local search algorithm that solves regularized GAP (7)-(8) with $\beta > 0$ using GAP algorithm in Section 3.1 as a subprocedure. Assume that \mathcal{L} is the current set of possible models³. Let \mathcal{L}_c be an arbitrary subset of \mathcal{L} and $\mathcal{M}_f(\mathcal{L}_c)$ denote the GAP solution when the label space is restricted to \mathcal{L}_c . Note that GAP ignores the label cost term in (7) but we could easily evaluate energy (7) for $\mathcal{M}_f(\mathcal{L}_c)$. The proposed LS-GAP algorithm greedily searches over different subsets \mathcal{L}_c for one such that $\mathcal{M}_f(\mathcal{L}_c)$ has the lowest value of energy (7). Our motivation to search for minima of energy (7)-(8) only among GAP solutions comes from an obvious observation that a global minima of (7)-(8) must also solve the GAP if the label space is restricted to a right subset of \mathcal{L} .

We define sets of all possible *add*, *delete* and *swap* combinatorial search moves as

$$\begin{aligned} \mathcal{N}^a(\mathcal{L}_c) &= \cup_{h \in \mathcal{L} \setminus \mathcal{L}_c} \{\mathcal{L}_c \cup h\} \\ \mathcal{N}^d(\mathcal{L}_c) &= \cup_{h \in \mathcal{L}_c} \{\mathcal{L}_c \setminus h\} \\ \mathcal{N}^s(\mathcal{L}_c) &= \cup_{\substack{h \in \mathcal{L}_c \\ \ell \in \mathcal{L} \setminus \mathcal{L}_c}} \{\mathcal{L}_c \cup \ell \setminus h\}. \end{aligned}$$

These are three different local neighbourhoods around \mathcal{L}_c . We also define a larger neighbourhood \mathcal{N}^* around \mathcal{L}_c which is the union of the above

$$\mathcal{N}^*(\mathcal{L}_c) = \mathcal{N}^a(\mathcal{L}_c) \cup \mathcal{N}^d(\mathcal{L}_c) \cup \mathcal{N}^s(\mathcal{L}_c).$$

LS-GAP uses a combination of *add*, *delete* and *swap* moves, as in [22], to greedily find a set of labels near current set \mathcal{L}_t that is better w.r.t. energy (7).

³In practice, \mathcal{L} is restricted to be the set of models that are assigned to at least one matched pair of features in energy (6) solution.

LS-GAP

```

 $\mathcal{L}_t \leftarrow \phi$ 
 $\mathcal{N}_t \leftarrow \mathcal{N}^*(\mathcal{L}_t)$ 
while  $\exists \mathcal{L}_c \in \mathcal{N}_t$ 
  if energy (7) of  $\mathcal{M}_f(\mathcal{L}_c) <$  energy (7) of  $\mathcal{M}_f(\mathcal{L}_t)$ 
     $\mathcal{L}_t \leftarrow \mathcal{L}_c$ 
     $\mathcal{N}_t \leftarrow \mathcal{N}^*(\mathcal{L}_t)$ 
  else
     $\mathcal{N}_t \leftarrow \mathcal{N}_t \setminus \mathcal{L}_c$ 
return the GAP solution  $\mathcal{M}_f(\mathcal{L}_t)$ 

```

In LS-GAP, we initially set \mathcal{L}_t to ϕ but it could be any arbitrary subset of \mathcal{L} . Then $\mathcal{N}^*(\mathcal{L}_t)$ is searched for a move with a GAP solution $\mathcal{M}_f(\mathcal{L}_c)$ of a lower energy (7) than the current one, i.e. $\mathcal{M}_f(\mathcal{L}_t)$. Such a move is accepted if it exists and \mathcal{L}_t is updated accordingly otherwise LS-GAP terminates. LS-GAP will definitely converge since energy (7) is lower bounded and \mathcal{L} is finite.

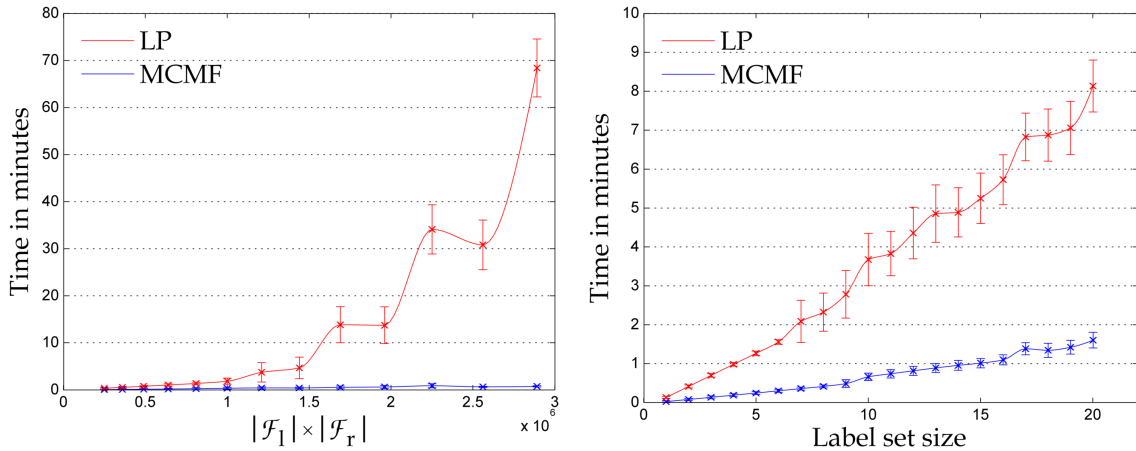
The subprocedure used in solving GAP is the bottle neck of LS-GAP. Figure 2 compares two LS-GAP implementations; the first uses Mosek [23] to solve the relaxed LP of the *integral linear program* and the other solves GAP using the fast GAP solver introduced in Section 3.1. Figure 2 shows that the MCMF based implementation (fast GAP solver) outperformed the LP one in the cases of fixed $|\mathcal{L}|$ and increasing number of features, and fixed number of features and increasing $|\mathcal{L}|$.

3.3 Label Constrained-GAP (LC-GAP)

LC-GAP solves a GAP instance with fixed labeling f , i.e. each left feature p must be assigned to a predefined model f_p . LC-GAP uses a slightly different graph construction than \mathcal{G}^* that enforces the required labeling constraints. The graph construction corresponding to a GAP instance under labeling f constraints is $\mathcal{G}_f^* = (\mathcal{V}, \mathcal{E})$ where

$$\begin{aligned}
 \mathcal{V} = & \{s, t\} \cup \{n_p | \forall p \in \mathcal{F}_l\} \\
 & \cup \{n_q | \forall q \in \mathcal{F}_r\} \cup \{n_{pf_p} | \forall p \in \mathcal{F}_l\} \\
 & \cup \{n_{qh} | \forall q \in \mathcal{F}_r, h \in \mathcal{L}\}
 \end{aligned}$$

and \mathcal{E} , capacity function u and cost function c are as defined as in \mathcal{G}^* provided that both edge nodes exist in \mathcal{V} of \mathcal{G}_f^* , see example in Fig. 1(b).



(a) LS-GAP performance for increasing number of possible matches (b) LS-GAP performance for increasing $|\mathcal{L}|$

Figure 2: Figures (a-b) show the average performance, over 50 runs of randomly generated GAP instances, of the LP and MCMF based implementation of LS-GAP. Figure (a) shows average performance for $|\mathcal{L}| = 5$ and increasing number of possible features $|\mathcal{F}_l| \times |\mathcal{F}_r|$ where $|\mathcal{F}_r| = |\mathcal{F}_l|$. Figure (b) shows average performance for $|\mathcal{F}_l| = |\mathcal{F}_r| = 10^3$ and increasing $|\mathcal{L}|$.

4 Ground truth

The ground truth is computed by first manually identifying and segmenting regions corresponding to separate models (planes/homographies), see Fig. 3. Then, we compute an optimal matching of extracted features inside each identified pair of corresponding regions with respect to the geometric fitting error and appearance. This method is similar to the one used in [20, 19].

Below we describe our technique for computing the “ground truth matching” for each model with manually identified spatial support, as illustrated in Fig. 3. We compute sets of SIFT features S_l and S_r inside each pair of manually identified corresponding regions, see Fig. 4. It is possible to independently fit one homography to each pair of corresponding sets $\{S_l, S_r\}$. For simplicity, we first assume that there are no occlusions, i.e if a feature appears in the left image then its corresponding feature appears in the right image and vice versa. Thus, the number of left image features equals the number of right image features. We will show how to deal with occlusions later.

The SIFT features of two corresponding sets, namely S_l and S_r see Fig. 4, are matched using the criteria described in [18]. Then we use RANSAC [24] to find a

homography θ_h that maximizes the number of inliers between the features in two corresponding regions. Using RANSAC in this case is not problematic since features in S_l and S_r support only one homography/model. This homography is only used as an initial guess in finding the ground truth model.

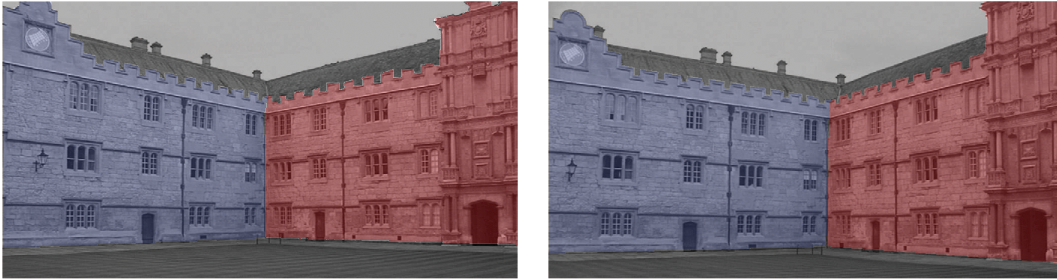
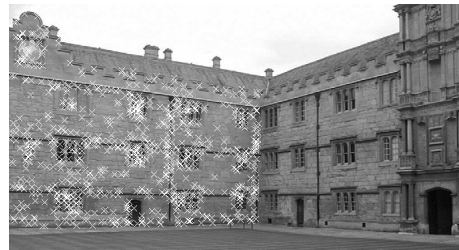
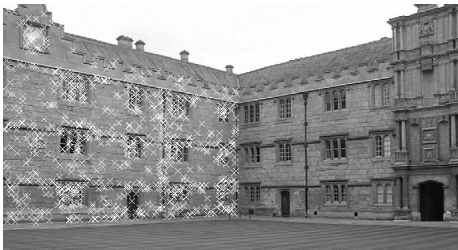
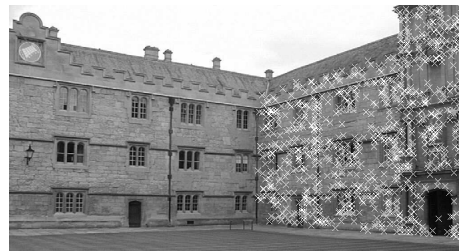


Figure 3: In this example we identified only two planes. The manually identified corresponding support regions for these two models are shown in blue and red.



(a) Example of corresponding sets S_l and S_r supporting the blue model in Fig. 3.



(b) Example of corresponding sets S_l and S_r supporting the red model in Fig. 3.

Figure 4: Two examples of the corresponding sets of features S_l and S_r supporting the blue (a) and red (b) models.

Given a homography θ_h , the problem of finding an optimal one-to-one matching that minimizes the total sum of matching scores between the left and right features

in two corresponding regions could be formulated as an assignment problem

$$\begin{aligned}
 \mathbf{AP} : \quad & \arg \min_{\mathcal{M}} \sum_{p \in S_l} \sum_{q \in S_r} D_{pq}(\theta_h) x_{pq} & (11) \\
 \text{s.t.} \quad & \sum_{p \in S_l} x_{pq} = 1 & \forall q \in S_r \\
 & \sum_{q \in S_r} x_{pq} = 1 & \forall p \in S_l \\
 & x_{pq} \in \{0, 1\} & \forall p \in S_l, \forall q \in S_r.
 \end{aligned}$$

The two linear constraints in AP enforce one-to-one correspondence between the features in S_r and S_l , see Fig. 5(a).

For any fixed matching \mathcal{M} the appearance term $\sum_{p \in S_l} \sum_{q \in S_r} Q(p, q) x_{pq}$ in AP's objective function becomes constant. After finding an optimal \mathcal{M} for AP, we could further decrease the objective value by re-estimating homography θ_h minimizing the geometric error, e.g. see first term in (2), over all the currently matched features. We can continue to iteratively re-estimate matching \mathcal{M} and homography θ_h until the objective value of AP could not be reduced anymore.

The described optimization procedure maybe sensitive to the initial homography found by RANSAC. In an effort to reduce such sensitivity we repeat the whole procedure several times, and report as ground truth matching \mathcal{M} and model θ_h that have the lowest value of the objective function of AP.

Now we can discuss possible occlusions that we ignored so far. The presence of occlusions or outliers introduces two problems. First, the number of features in corresponding regions are no longer guaranteed to be the same. Such an imbalance between the features has to be addressed in order to enforce one-to-one correspondence. Second, we can no longer assume that there exists one homography that fits all features.

To balance out any possible difference between the sizes of sets S_l and S_r we use dummy features with a constant matching cost penalty, as detailed below. Without loss of generality we can assume that the number of extracted features in the left region is less than or equal to those in the right region⁴. In this case, there are at least $|S_r| - |S_l|$ occluded features in the right image. As illustrated in Fig. 5(b), an imbalance between the number of features renders the one-to-one correspondence constraints in AP infeasible. One way to overcome this problem is to add $|S_r| - |S_l|$ dummy features to set S_l , see Fig. 5(c). We define a fixed matching cost penalty $D_{dq} = T$ for assigning any dummy feature d to any q in S_r . It is also possible to use

⁴We could always swap the regions to satisfy that assumption as long as the used geometric error and appearance measures are symmetric.

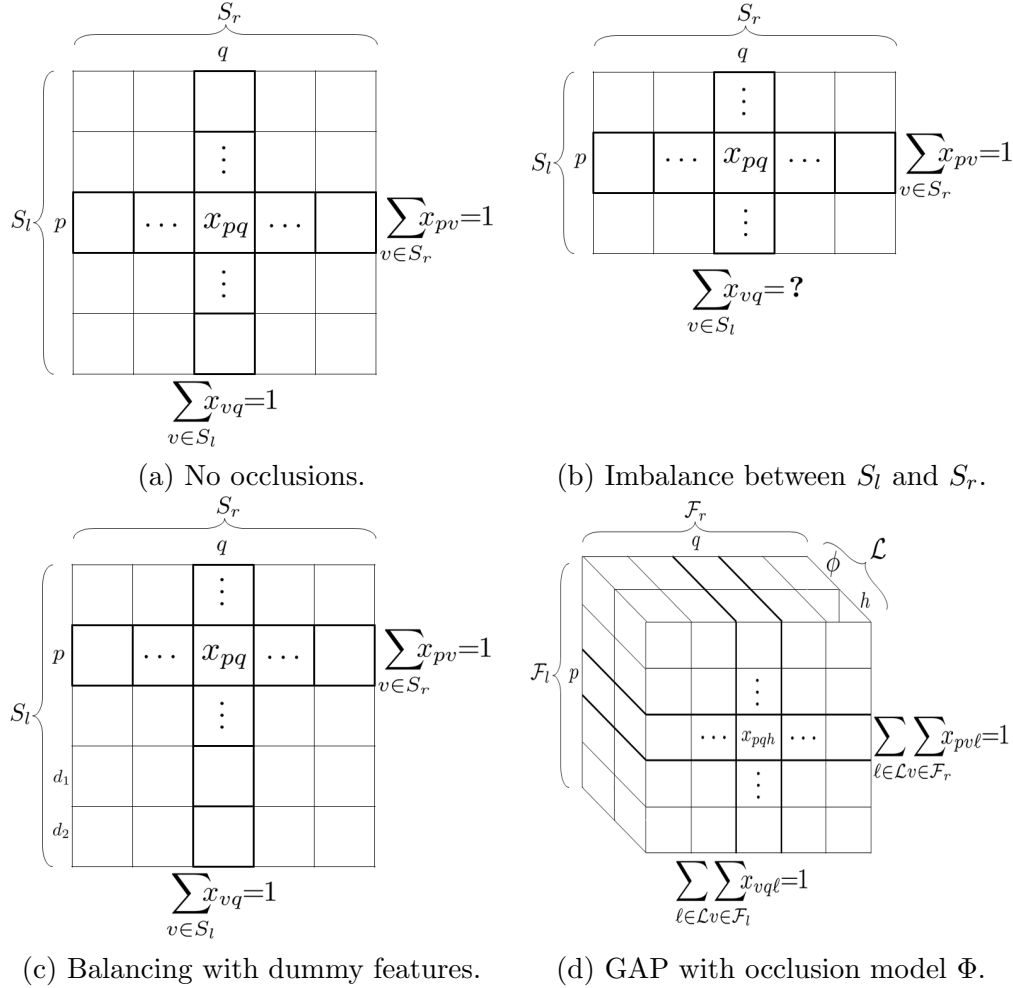


Figure 5: Figure (a) shows the straight forward case, no occlusions, for enforcing the one-to-one correspondences. Notice that in this case the number of features in both images is the same and therefore the one-to-one correspondences constraints are balanced. Figure (b) shows a case with unbalanced one-to-one correspondence constraints, i.e there are no enough features in S_l to enforce the one-to-one correspondence constraints. And, figure (c) shows how to balanced the one-to-one correspondence constraints by introducing the dummy feature d . Figure (d) shows how to account for occlusions, using occlusion model ϕ , in case of balanced one-to-one correspondence constraints.

only one dummy feature d in S_l but for that specific feature constraint $\sum_{q \in S_r} x_{dq} = 1$ would have to be replaced by $\sum_{q \in S_r} x_{dq} = |S_r| - |S_l \setminus \{d\}|$. We adapt the first approach with multiple dummy features only to simplify our notation and avoid the special handling of feature d . The use of dummy feature/entity is a common technique for balancing out unbalanced assignment problems in operations research [25].

Even under the assumption that $|S_l| = |S_r|$ occlusions are possible and we can not assume that there exists a homography that fits all features. In order to make our approach robust to occlusions/outliers we use generalized the assignment problem, GAP, to allow each feature to choose between two models: a homography θ_h and an occlusion model ϕ such that $D_{pq}(\phi) = T$ for any $p \in S_l$ and $q \in S_r$. The use of an occlusion (or outlier) model with a uniformly distributed matching cost is a fairly common technique in Computer Vision [16, 21], see Fig. 5(d).

5 Evaluation

In this section, we compare the matching quality of the EFM framework vs. standard SIFT matching [18]. Then we discuss some of the EFM framework properties, e.g. convergence rate and the effect of the initial set of proposals size on the matching quality. Finally, we compare the quality of the estimated models by the EFM framework to the models estimated by an EF algorithm PEARL[16].

Our matching evaluation criterion is based on Receiver Operating Characteristics (ROC) of the True Positive Rate (TPR) vs. the False Positive Rate (FPR). The ROC attributes for matching \mathcal{M} and ground truth (GT) matching \mathcal{M}_{GT} are defined as follows:

Positive (P) number of matches identified by \mathcal{M}_{GT}

Negative (N) number of potential matches that were rejected by \mathcal{M}_{GT} ,

$$\text{i.e. } N = |\mathcal{F}_l| \times |\mathcal{F}_r| - P$$

True Positive (TP) number of matches identified by \mathcal{M} and \mathcal{M}_{GT} (intersection)

False Positive (FP) number of matches identified by \mathcal{M} but were rejected by \mathcal{M}_{GT}

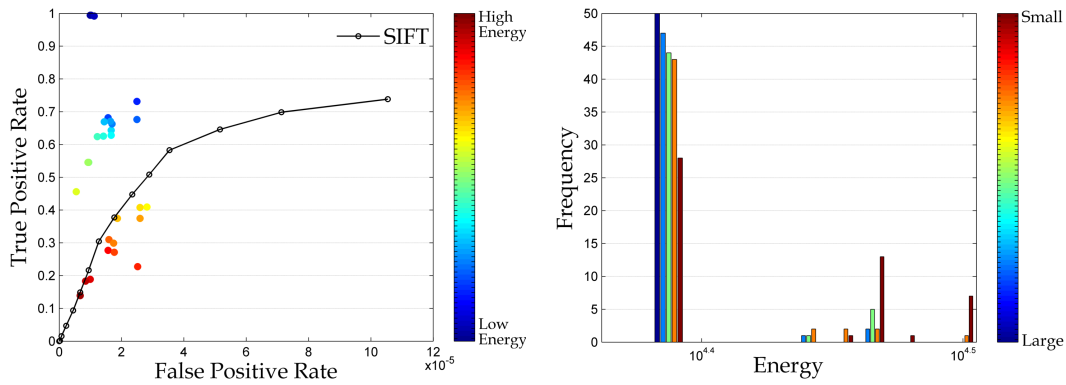
True Positive Rate (TPR) $\frac{TP}{P}$

False Positive Rate (FPR) $\frac{FP}{N}$.

Figure 6(a) shows the ROC curve of standard SIFT matching achieved by varying the second best ratio (SBR) threshold where SBR is the ratio of distance between a left feature descriptor and the closest right features descriptor to the distance of the second closest. EFM is non-deterministic and the energy of convergence, a.k.a final energy, depends on the size of initial set of proposals $|\mathcal{L}|$. Therefore, for EFM we

show a scatter plot that relates the ROC attributes to the final energy (color coded) by varying $|\mathcal{L}|$. As can be see, EFM outperforms standard SIFT matching and the lower the final energy the better the matching quality. Furthermore, Fig. 6(b) shows multiple histograms relating the final energy frequencies, of 50 runs, to $|\mathcal{L}|$ (color coded). As can be seen, the bigger $|\mathcal{L}|$ is the more likely the final energy is going to be small and the more likley that EFM behaviour becomes more deterministic over different runs.

Figure 7 shows the effect of EFM iterations on the energy with respect to time for different $|\mathcal{L}|$. For each $|\mathcal{L}|$ the experiment is repeated 50 times. On the average each iteration took 1.5 mins, and most of the energy was reduced in the first three iterations. EFM converged on the average after 5 iterations. The plots in Fig. 6 and 7 are shown for the Metron College example, in Fig. 8, to illustrate the general characteristics/behavior of our method. It will be meaningless to average these plots over multiple examples since they would not share the same energy scale, i.e. a low energy for one example could be high for another one.



(a) EFM vs SIFT matching quality

(b) Effect of $|\mathcal{L}|$ on the final energy

Figure 6: Figure (a) shows the ROC curve of the standard SIFT matches by varying the SBR threshold, and the scatter plot represents EFM results for different sizes of initial set or proposals. The scatter plot is color coded to show relation between the achieved final energy and the quality of the matching, the lower the energy (blue) the better the matching. Figure (b) shows multiple histograms of the final energies for different sizes of initial set of proposals—blue indicates a large initial set of proposals while red indicates a small set. The larger the size of the initial set of proposals the more likely that EFM will converge to a low energy.

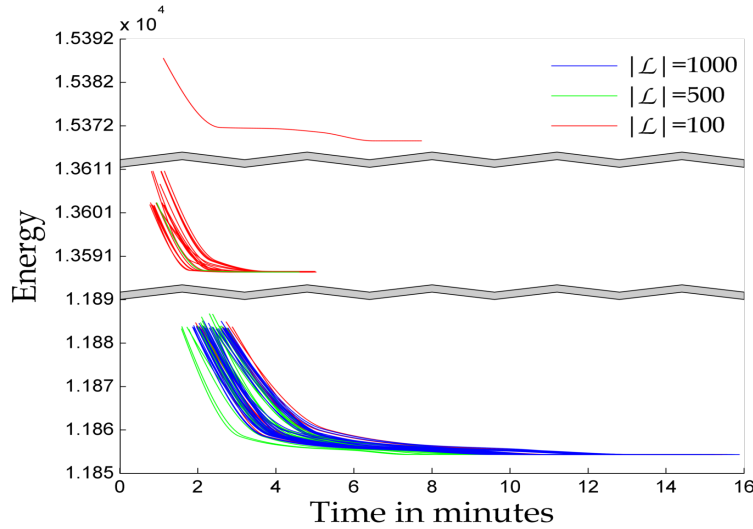


Figure 7: EFM energy over time in minutes. EFM converges on the average in 5 iterations, and an iteration on the average takes 1.5 minutes.

Figures 8(a) and (b) show left features of EF [16] inliers and left features of matches identified by EFM, respectively. Also, outliers or unmatched features are shown as x. EFM on the average found double the number of matches compared to using EF and SIFT standard matching. Figures 8(c) and (d), and (e) and (f) are the zoom in for Segment 1 and Segment 2 in (a) and (b), respectively. Figures 8(g) and (h) show the matching, over a small region, between the left and right images results of EF and EFM, respectively.

Figure 9 shows more results comparing EFM vs. EF and SIFT standard matching. In general EFM was able to find more matches than EF but EFM outperformed EF in two particular examples; the graphite example, shown in second row, in which large viewpoint between left and right images resulted in SIFT standard matching producing only 76 potential matches, and redbrick house example, shown in third row, in which repetitive texture of the bricks reduced the discriminate power of SIFT descriptor.

In order to evaluate the quality of the estimated model θ_h , we will use the following geometric error ratio $GQ(\theta_h)$

$$GQ(\theta_h) := \frac{STE(\theta_h, f_{GT}, \mathcal{M}_{GT})}{STE(\theta_{GT}, f_{GT}, \mathcal{M}_{GT})}$$

where f_{GT} is the ground truth labeling and $STE(\theta_h, f, \mathcal{M})$ is the Symmetric Transfer Error of θ_h , i.e. geometric error, computed for labeling f and matching \mathcal{M} —the close

$GQ(\theta_h)$ is to 1 the better the model estimate.

Table 1 shows the effect of increasing viewpoint angle, between the left and right images, on the quality of model estimates. As the viewpoint increases the number of matched points by EF sharply decreases while for EFM the decrease is not as steep. In addition, EF becomes more sensitive to the used SBR threshold for increasing viewpoint, see variance for large viewpoint. Furthermore, EFM archives near optimal matching, see TRP and FPR.

The used fitting threshold T affects the ground truth, EFM and EF results, as it is a parameter for these methods. Table 2 shows the effect of increasing T on EF and EFM. For the case of $T \leq 1$, T is underestimated and running the ground truth multiple times will result in similar final energies but slightly different matching. The more we decrease T the more different the matchings will be. For $T \leq 2$ and $T \leq 3$ the ground truth result become more deterministic over multiple runs. Finally, when computing the ground truth for all the examples shown above we manually handed tuned T to find the smallest T that gives a stable ground truth over multiple runs.

6 Conclusions

We introduced two energy functionals that use different regularizers for the *fit- \mathcal{E} -match* problem. We also introduced optimization frameworks for these functionals. Our experimental results show that our energy-based *fit- \mathcal{E} -match* framework finds a near optimal solution for the feature-to-feature matching and better model estimates in contrast to state-of-the-art energy-based fitting frameworks, e.g. PEARL. In addition, we showed that for a given set of models it is possible to efficiently find the optimal feature-to-feature matching and match-to-label assignment. Our framework could be used to *fit- \mathcal{E} -match* more complex models, e.g. fundamental matrices, without affecting the framework’s complexity. It could also be used to *fit- \mathcal{E} -match* a mixture of different models, e.g. homographies and affine transformations, and penalize each model/label based on its complexity. Finally, we plan on applying our framework to estimate camera pose.

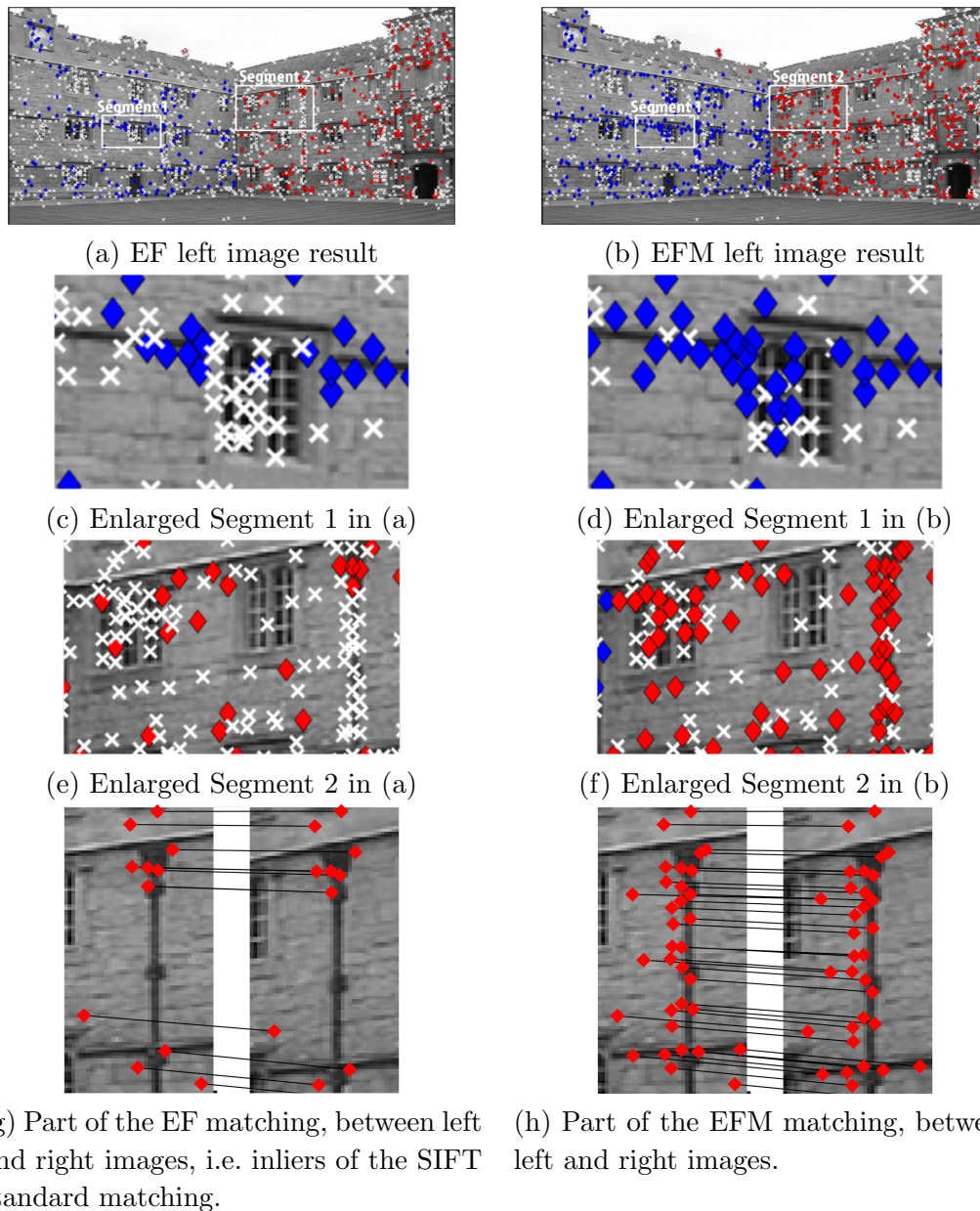


Figure 8: Metron College from VGG Oxford, Fig. (a) shows EF result (average TPR=0.51 and FPR=1.6E-05) and (b) shows EFM result (average TPR=0.98 and FPR=9.1E-06). The averaging is done over 50 runs. Figures (c-d) show the enlargement of Segment 1 in (a) and (b), respectively, and Fig. (e-f) show the enlargement of Segment 2 in (a) and (b), respectively. Figures (g-h) show the matching, between two small regions in the left and right images, of the EF and EFM results, respectively. The average GQ ratios are 1.042 and 1.0630 for EF estimated models, and 1.0102 and 1.0079 for EFM estimated models.

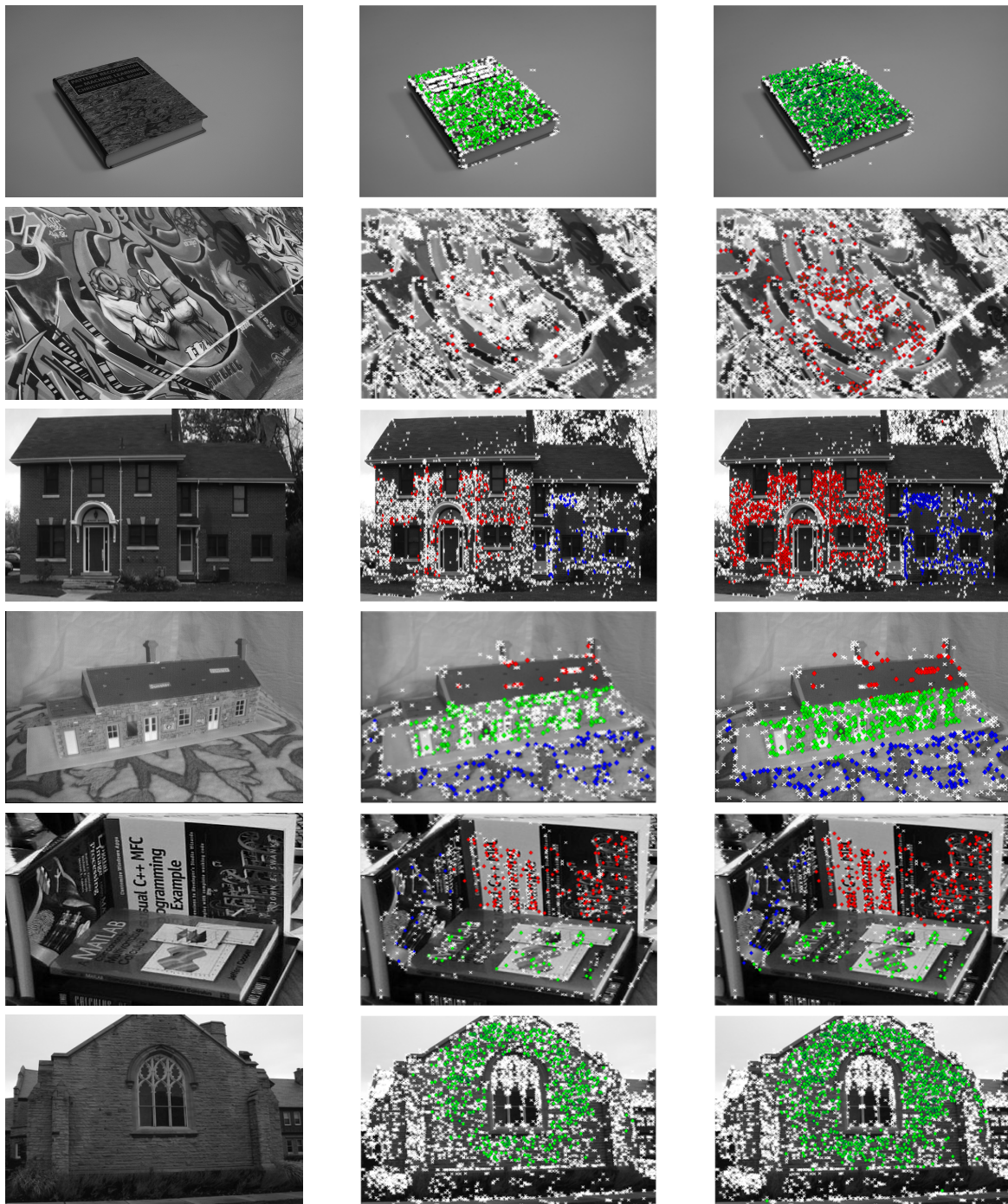


Figure 9: First column shows left images of the examples, second and third columns show the EF and EFM results, respectively. The average increase, over 50 runs, in the number of matches found by EFM in comparison to EF for the examples shown above (top to bottom) is 0.76, 10.53, 3.33, 0.44, 0.6 and 0.68, respectively.

| | | GQ | | | ROC | | | |
|------------------|---------------|---------------|--------|----------|-----|-------|-------------|-----------------|
| | | median | mean | variance | TP | FP | TPR | FPR |
| small viewpoint | EFM | 1.0048 | 1.0074 | 4.00E-06 | 824 | 18.08 | 0.98 | 2.30E-06 |
| | EF SBR=0.6 | 1.0386 | 1.0475 | 1.00E-03 | 602 | 31.66 | 0.72 | 4.10E-06 |
| | EF SBR=0.7 | 1.0415 | 1.0519 | 1.30E-03 | 652 | 41.14 | 0.78 | 5.20E-06 |
| | EF SBR=0.8 | 1.0460 | 1.0521 | 8.00E-04 | 691 | 51.60 | 0.82 | 6.60E-06 |
| medium viewpoint | EFM | 1.0183 | 1.0194 | 1.00E-06 | 501 | 26.96 | 0.97 | 3.10E-06 |
| | EF SBR=0.6 | 1.1742 | 1.3031 | 1.71E-01 | 94 | 19.18 | 0.18 | 2.20E-06 |
| | EF SBR=0.7 | 1.1989 | 1.3012 | 8.64E-02 | 171 | 33.22 | 0.33 | 3.80E-06 |
| | EF SBR=0.8 | 1.0806 | 1.2594 | 1.09E-00 | 256 | 49.20 | 0.49 | 5.6E-06 |
| large viewpoint | EFM | 1.0523 | 1.0698 | 2.00E-03 | 300 | 15.72 | 0.96 | 1.70E-06 |
| | EF SBR=0.6 | 2.6412 | 2.6413 | 1.30E-06 | 9 | 2 | 0.03 | 2.20E-07 |
| | EF SBR=0.7 | 1.8993 | 2.2440 | 1.22E-00 | 19 | 5.48 | 0.06 | 5.90E-07 |
| | EF SBR=0.8 | 2.4915 | 3.8799 | 9.31E-00 | 36 | 13.04 | 0.12 | 1.40E-06 |
| multi-model case | EFM | 1.0102 | 1.0102 | 1.90E-09 | 656 | 36.49 | 0.98 | 9.10E-06 |
| | | 1.0046 | 1.0079 | 1.20E-05 | | | | |
| | EF SBR=0.6 | 1.0625 | 1.0681 | 7.00E-04 | 258 | 45.48 | 0.38 | 1.10E-05 |
| | | 1.0397 | 1.0514 | 1.80E-03 | | | | |
| | EF SBR=0.7 | 1.0383 | 1.0420 | 2.00E-04 | 344 | 63.04 | 0.52 | 1.60E-05 |
| | | 1.0427 | 1.0630 | 2.20E-03 | | | | |
| | EF SBR=0.8 | 1.0218 | 1.0243 | 3.00E-04 | 431 | 76.18 | 0.64 | 1.90E-05 |
| | | 1.0447 | 1.0905 | 9.80E-03 | | | | |

Table 1: In the case of a single model and increasing viewpoint (Graphite VGG Oxford), the first three blocks show the average, over 50 runs, ROC attributes and GQ of EFM and EF (using different SBR ratios). The EFM and EF results were comparable for small viewpoint but as the viewpoint increases EFM model estimates becomes more reliable in comparison to EF estimates. The last block shows the results for a multi-model case (Metron College VGG Oxford). In both cases, EFM achieved near optimal matching.

| | | GQ | | | ROC | | | |
|------------|---------------|--------|--------|----------|-----|--------|------|---------|
| | | median | mean | variance | TP | FP | TPR | FPR |
| $T \leq 1$ | EFM | 1.0031 | 1.0040 | 6.3E-6 | 529 | 34.20 | 0.95 | 8.5E-06 |
| | | 1.0225 | 1.1251 | 0.0207 | | | | |
| | EF SBR=0.7 | 1.1999 | 1.2470 | 0.0427 | 241 | 33.12 | 0.43 | 8.3E-06 |
| | | 1.2384 | 1.2750 | 0.0331 | | | | |
| $T \leq 2$ | EFM | 1.0102 | 1.0102 | 1.9E-9 | 656 | 36.489 | 0.98 | 9.1E-06 |
| | | 1.0046 | 1.0079 | 1.2E-5 | | | | |
| | EF SBR=0.7 | 1.0383 | 1.0427 | 0.0002 | 344 | 63.04 | 0.52 | 1.6E-05 |
| | | 1.0427 | 1.0630 | 0.0022 | | | | |
| $T \leq 3$ | EFM | 1.0084 | 1.0083 | 0.4E-9 | 720 | 45 | 0.99 | 1.1E-05 |
| | | 1.0046 | 1.0079 | 1.2E-5 | | | | |
| | EF SBR=0.7 | 1.0372 | 1.0347 | 2.5E-5 | 369 | 65.34 | 0.51 | 1.6E-05 |
| | | 1.0500 | 1.0589 | 0.0015 | | | | |

Table 2: shows the effect of the fitting threshold T (used in computing ground truth, EF and EFM) on the average quality of estimated models and ROC attributes, over 50 runs. The performance for both EF and EFM in the case of $T \leq 2$ is better than the case of $T \leq 1$ because the threshold in the later case is underestimated—see GQ variance. Furthermore, the average increase in the model estimate quality for EF and EFM between $T \leq 3$ and $T \leq 2$ is not as significant as the average increase between $T \leq 2$ and $T \leq 1$.

A Lemma 3.1 Proof

The following proof assumes that there exists a feasible solution for GAP with a finite objective value. GAP is unfeasible when $|\mathcal{F}_l| \neq |\mathcal{F}_r|$, e.g. $|\mathcal{F}_l| < |\mathcal{F}_r|$ and in that case adding $(|\mathcal{F}_r| - |\mathcal{F}_l|)$ dummy features with a fixed matching penalty T to \mathcal{F}_l will ensure the GAP feasibility. The objective value of a feasible GAP solution is guaranteed to be finite when GAP is solved over any set of models and an outlier model ϕ with a fixed matching penalty T for all possible pairs of matched features. We will prove a more general theorem than Lemma 3.1. Lemma 3.1 is a derivative of Theorem A.1.

Theorem A.1 *“There exists an optimal solution, with an objective value k^* , of a GAP instance if and only if there exists a valid MCMF \mathbf{F}^* over \mathcal{G}^* , of the GAP instance, with $\text{cost}(\mathbf{F}^*) = k^*$ ”.*

Proof Assume that there exists a GAP optimal solution \mathcal{M}_f^* with an objective value k^* . If there exists a valid MCMF \mathbf{F} over \mathcal{G}^* with $\text{cost}(\mathbf{F}) = k$ such that $k < k^*$ then we can construct a feasible GAP solution \mathcal{M}_f where $\mathcal{M}_f = \{x_{pqh} = \mathbf{F}(n_{ph}, n_{qh}) \mid p \in \mathcal{F}_l, q \in \mathcal{F}_r, h \in \mathcal{L}\}$. Using Corollary A.2 we can deduce that the objective value of the constructed GAP solution \mathcal{M}_f is equal to $\text{cost}(\mathbf{F})$. Now we prove that the constructed solution \mathcal{M}_f is feasible by showing that \mathcal{M}_f can not be unfeasible, i.e. one or more of the constraints (8) can not be violated in the constructed solution. Constraints (8) are violated when

I *a feature $p \in \mathcal{F}_l$ is not assigned to any feature.*

That means the MCMF \mathbf{F} used to construct \mathcal{M}_f does not saturate \mathcal{G}^* and this is a contradiction to our assumption that \mathbf{F} is a MCMF. Notice edges (s, n_p) for $p \in \mathcal{F}_l$ must be saturated as in the worst case scenario p will be matched to another feature through the outlier model for a fixed cost penalty T .

II *a feature $p \in \mathcal{F}_l$ is assigned to more than one feature in \mathcal{F}_r , e.g. q_1 and q_2 .*

If there exist two models h and ℓ such that $x_{pq_1h}=1$ and $x_{pq_2\ell}=1$ then $\mathbf{F}(n_{ph}, n_{q_1h})=1$ and $\mathbf{F}(n_{p\ell}, n_{q_2\ell})=1$ must be true by construction of \mathcal{M}_f . By construction of \mathcal{G}^* , n_{ph} and $n_{p\ell}$ acquire their flow from n_p , and n_p could only push out one unit of flow. Therefore, for $\mathbf{F}(n_{ph}, n_{q_1h}) = 1$ and $\mathbf{F}(n_{p\ell}, n_{q_2\ell}) = 1$ to be true n_p must push two units of flow and that contradicts our assumption that \mathbf{F} is a valid flow over \mathcal{G}^* .

III *a feature $q \in \mathcal{F}_r$ is assigned to a zero or more than one feature in \mathcal{F}_l .*

We could show that scenario could not happen for \mathcal{M}_f by reversing the roles of p and q in I and II.

IV a matched pair of features p and q are assigned to more than one model. e.g. h_1 and h_2 .

If $x_{pqh_1} = 1$ and $x_{pqh_2} = 1$ then $\mathbf{F}(n_{ph_1}, n_{qh_1}) = 1$ and $\mathbf{F}(n_{ph_2}, n_{qh_2}) = 1$ must be true by construction of \mathcal{M}_f . By construction of \mathcal{G}^* , n_{ph_1} and n_{ph_2} acquire two units flow from n_p while n_p could only push out one unit of flow. Therefore, for $\mathbf{F}(n_{ph_1}, n_{qh_1}) = 1$ and $\mathbf{F}(n_{ph_2}, n_{qh_2}) = 1$ to be true n_p must push out two units of flow and that contradicts our assumption that \mathbf{F} is a valid flow over \mathcal{G}^* .

Finally, if such a solution \mathcal{M}_f exist then \mathcal{M}_f^* is not optimal as k^* will be bigger than k and that contradicts our main assumption that \mathcal{M}_f^* an optimal GAP solution, i.e. k^* is the lowest possible objective value.

Assume that \mathbf{F}^* is a valid MCMF over \mathcal{G}^* with $cost(\mathbf{F}^*) = k^*$. If there exists an feasible solution \mathcal{M}_f for which the objective value is $k < k^*$ then we can consturct a valid MCMF \mathbf{F} where

$$\begin{aligned} \mathbf{F}(s, n_p) &= 1 && \forall p \in \mathcal{F}_l \\ \mathbf{F}(n_p, n_{ph}) &= \begin{cases} 1 & \exists q \in \mathcal{F}_r \text{ where } x_{pqh} = 1 \\ 0 & \text{otherwise} \end{cases} && \forall p \in \mathcal{F}_l, h \in \mathcal{L} \\ \mathbf{F}(n_{ph}, n_{qh}) &= x_{pqh} && \forall p \in \mathcal{F}_l, q \in \mathcal{F}_r, h \in \mathcal{L} \\ \mathbf{F}(n_{qh}, n_q) &= \begin{cases} 1 & \exists p \in \mathcal{F}_l \text{ where } x_{pqh} = 1 \\ 0 & \text{otherwise} \end{cases} && \forall q \in \mathcal{F}_r, h \in \mathcal{L} \\ \mathbf{F}(n_q, t) &= 1 && \forall q \in \mathcal{F}_r. \end{aligned}$$

Using Corollary A.2 we can deduce that the $cost(\mathbf{F}) = k$.

No we will prove that the constructed flow \mathbf{F} is a valid MCMF. A flow is considered valid if it satisfies the capacity and conservation of flow constraints over \mathcal{G}^* . \mathbf{F} satisfies the capacity constraints by construction of \mathbf{F} —the flow through any edge is either 1 or 0 while all edge capacities are 1. Furthermore, \mathbf{F} was constructed in a way that preserves the flow with in \mathcal{G}^* . That is, if there is a flow through edge (n_{ph}, n_{qh}) we create a flow from s to n_{ph} and from n_{qh} to t along the following paths $\{s, n_p, n_{ph}\}$ and $\{n_{qh}, n_q, t\}$, respectively. Therefore, the conservation flow is preserved at n_{ph}, n_{qh}, n_p and n_q . Notice that there can not exist n_{ph_1} and n_{ph_2} both creating along $\{s, n_p, ph_1\}$ and $\{s, n_p, ph_2\}$ as in this case \mathcal{M}_f will unfeasible which is a contradiction. Moreover, the amount of flow going in to \mathcal{G}^* through s is $|\mathcal{F}_l|$ and the amount of flow going out of \mathcal{G}^* through t is $|\mathcal{F}_r|$ and since \mathcal{M}_f is a feasible GAP solution, by definition, then $|\mathcal{F}_l|$ must be equal to $|\mathcal{F}_r|$. Thus, the conservation of flow constraint is preserved at s and t , and \mathcal{G}^* is saturated. Thus, the constructed flow \mathbf{F} is a valid MCMF flow.

Finally, if such a solution \mathbf{F} exist then \mathbf{F}^* is not MCMF as $cost(\mathbf{F}) < cost(\mathbf{F}^*)$ and that contradicts our main assumption that \mathbf{F}^* is a MCMF over \mathcal{G}^* .

Corollary A.2 For a valid \mathbf{F} over \mathcal{G}^* and a GAP solution \mathcal{M}_f where $\mathcal{M}_f = \{x_{pqh} = \mathbf{F}(n_{ph}, n_{qh}) \mid p \in \mathcal{F}_l, q \in \mathcal{F}_r, h \in \mathcal{L}\}$, the objective value of the GAP solution \mathcal{M}_f is equal to $\text{cost}(\mathbf{F})$.

Proof

$$\begin{aligned}
\text{cost}(\mathbf{F}) &= \sum_{(v,w) \in \mathcal{E}} c(v,w) \cdot \mathbf{F}(v,w) && \text{by definition of flow cost} \\
&= \sum_{(n_{ph}, n_{qh}) \in \mathcal{E}} c(n_{ph}, n_{qh}) \cdot \mathbf{F}(n_{ph}, n_{qh}) && \text{by construction of } \mathcal{G}^*, \text{ other edge costs are 0} \\
&= \sum_{(n_{ph}, n_{qh}) \in \mathcal{E}} D_{pq}(\theta_h) \cdot \mathbf{F}(n_{ph}, n_{qh}) && \text{by definition of } c \text{ over } \mathcal{E} \\
&= \sum_{\substack{p \in \mathcal{F}_l \\ q \in \mathcal{F}_r \\ h \in \mathcal{L}}} D_{pq}(\theta_h) \cdot x_{pqh} && \text{by condition in Corollary A.2.}
\end{aligned}$$

B Total Modularity Proof

Our generalization of the assignment problem for solving the matching problem over a set of models \mathcal{L} such that $|\mathcal{L}| \geq 1$ could be formulated as integer linear program

$$\begin{aligned}
\mathbf{GAP} : \quad & \arg \min_{\mathcal{M}_f} \quad \sum_{h \in \mathcal{L}} \sum_{p \in \mathcal{F}_l} \sum_{q \in \mathcal{F}_r} D_{pq}(\theta_h) x_{pqh} \\
& \text{s.t.} \quad \sum_{h \in \mathcal{L}} \sum_{p \in \mathcal{F}_l} x_{pqh} = 1 \quad \forall q \in \mathcal{F}_r \quad (12)
\end{aligned}$$

$$\sum_{h \in \mathcal{L}} \sum_{q \in \mathcal{F}_r} x_{pqh} = 1 \quad \forall p \in \mathcal{F}_l \quad (13)$$

$$x_{pqh} \in \{0, 1\} \quad \forall h \in \mathcal{L}, p \in \mathcal{F}_l, q \in \mathcal{F}_r.$$

The rest of this section proves that GAP is an *integral linear program*, that is, its LP relaxation is guaranteed to have an integer solution.

Let us denote the coefficient matrix and the right hand side vector of equations (12) and (13) by A and b , respectively. It is known [26] that a linear program with constraints $Ax = b$ is *integral* for any objective function as long as b is integer, which is true in our case, and matrix A is *totally unimodular*. It remains to prove that A is totally unimodular.

Lemma B.1 Coefficient matrix A of GAP's linear constraints is totally unimodular.

Proof The coefficient matrix A of GAP has a special structure that facilitates its proof of total unimodularity. Let us assume, without loss of generality, that the number of features on the left and right images is n . Then the coefficients matrix in case $\mathcal{L} = \{h\}$ could be written as follows

$$A' = \left(\begin{array}{ccc|ccc} x_{11h} & x_{1nh} & \dots & x_{n1h} & x_{nnh} & \\ \hline 1 & \dots & 1 & & & \\ & & \dots & & & \\ \hline 1 & & & 1 & \dots & 1 \\ & \ddots & & & \ddots & \\ & & & 1 & & 1 \end{array} \right) \left. \begin{array}{l} \vphantom{A'} \\ \vphantom{A'} \end{array} \right\} \begin{array}{l} \text{eqs (12)} \\ \text{eqs (13)} \end{array} .$$

In case $|\mathcal{L}| > 1$ then coefficients matrix A could be written as follows

$$A = \left(\begin{array}{c|c|c|c} 1 & 2 & \dots & |\mathcal{L}| \\ \hline A' & A' & \dots & A' \end{array} \right).$$

Heller and Tompkins [27] showed that in order to prove that A is totally unimodular it is sufficient to prove that the following three conditions are satisfied by the coefficient matrix:

I *Every entry of the coefficient matrix is either 0, +1, or -1.*

This condition is satisfied for A by construction, see equations (12) and (13).

II *Every column of the coefficient matrix contains at most two non-zero entries.*

Each column in A corresponds to a unique decision variable, for example x_{pqh} . Note that variable x_{pqh} appears only once in linear equations (12) and once in linear equations (13). Therefore, variable x_{pqh} appears twice in A . That is, the column corresponding to x_{pqh} has exactly two non-zero entries.

III *There exists a two set partitioning, say I_1 and I_2 , for the rows of the coefficients matrix such that if two non-zero entries in any column have the same sign then these two rows are in different sets. And, if the non-zero entries have different signs then these two rows belong to the same set.*

Notice that A' satisfies condition III by setting I_1 and I_2 to the rows of (12) and (13), respectively. Also, the coefficients matrix A in case of more than one model is simply the horizontal concatenation of the coefficients matrix A' to itself

$|\mathcal{L}|$ times. Thus, the constraints added over the two disjoint sets I_1 and I_2 , that satisfy condition III over A' , by repeating its columns are redundant. Finally, condition III will be satisfied by A by the same row partitioning that would satisfy condition III for A' .

References

- [1] B. Triggs, P. McLauchlan, R. Hartley, and A. Fitzgibbon, "Bundle adjustment - a modern synthesis," in *Vision Algorithms*, vol. LNCS 1883, pp. 298–372, Springer-Verlag, 2000.
- [2] M. Brown and D. G. Lowe, "Automatic panoramic image stitching using invariant features," *International Journal of Computer Vision (IJCV)*, vol. 74, pp. 59–73, August 2007.
- [3] T.-J. Chin, H. Wang, and D. Suter, "Robust fitting of multiple structures: The statistical learning approach," in *International Conference on Computer Vision (ICCV)*, 2009.
- [4] C. Tomasi and T. Kanade, "Shape and motion from image streams under orthography: a factorization method," *International Journal of Computer Vision (IJCV)*, 1992.
- [5] J. Costeira and T. Kanade, "A multi-body factorization method for motion analysis," in *ICCV*, 1995.
- [6] R. Vidal, R. Tron, and R. Hartley, "Multiframe motion segmentation with missing data using powerfactorization and GPCA," *International Journal of Computer Vision (IJCV)*, 2008.
- [7] P. David, D. Dementhon, R. Duraiswami, and H. Samet, "Softposit: Simultaneous pose and correspondence determination," *IJCV*, vol. 59, no. 3, pp. 259–284, 2004.
- [8] B. Tordoff and D. Murray, "Guided-mlesac: Faster image transform estimation by using matching priors," *Pattern Analysis and Machine Intelligence, IEEE Transactions on*, vol. 27, no. 10, pp. 1523–1535, 2005.
- [9] O. Chum and J. Matas, "Matching with prosac-progressive sample consensus," in *Computer Vision and Pattern Recognition, 2005. CVPR 2005. IEEE Computer Society Conference on*, vol. 1, pp. 220–226, IEEE, 2005.

- [10] T. Sattler, B. Leibe, and L. Kobbelt, "Scramsac: Improving ransac's efficiency with a spatial consistency filter," in *Computer Vision, 2009 IEEE 12th International Conference on*, pp. 2090–2097, IEEE, 2009.
- [11] L. Torresani, V. Kolmogorov, and C. Rother, "A dual decomposition approach to feature correspondence," *PAMI*, vol. 99, no. PrePrint, 2012.
- [12] A. Berg, T. Berg, and J. Malik, "Shape matching and object recognition using low distortion correspondences," in *CVPR*, pp. 26–33, 2005.
- [13] M. Leordeanu and M. Hebert, "A spectral technique for correspondence problems using pairwise constraints," in *ICCV*, pp. 1482–1489, 2005.
- [14] S. Gold and A. Rangarajan, "A graduated assignment algorithm for graph matching," *PAMI*, vol. 18, no. 4, pp. 377–388, 1996.
- [15] E. Serradell, M. Özuysal, V. Lepetit, P. Fua, and F. Moreno-Noguer, "Combining geometric and appearance priors for robust homography estimation," *Computer Vision–ECCV 2010*, pp. 58–72, 2010.
- [16] A. Delong, A. Osokin, H. Isack, and Y. Boykov, "Fast Approximate Energy Minimization with Label Costs," *International Journal of Computer Vision (IJCV)*, vol. 96, pp. 1–27, Jan. 2012.
- [17] A. V. Goldberg, "An efficient implementation of a scaling minimum-cost flow algorithm," *Journal of Algorithms*, vol. 22, pp. 1–29, 1992.
- [18] D. G. Lowe, "Distinctive image features from scale-invariant keypoints," *International Journal of Computer Vision (IJCV)*, vol. 60, no. 2, pp. 91–110, 2004.
- [19] K. Mikolajczyk and C. Schmid, "A performance evaluation of local descriptors," in *International Conference on Computer Vision & Pattern Recognition*, vol. 2, (Madison, United States), pp. 257–263, IEEE Computer Society, 2003.
- [20] T. Ke and R. Sukthankar, "Pca-sift: a more distinctive representation for local image descriptors," in *Proceedings of the 2004 IEEE computer society conference on Computer vision and pattern recognition*, (Washington, DC, USA), pp. 506–513, IEEE Computer Society, 2004.
- [21] H. N. Isack and Y. Boykov, "Energy-based Geometric Multi-Model Fitting," *International Journal of Computer Vision (IJCV)*, vol. 97, pp. 123–147, April 2012.

- [22] V. Arya, N. Garg, R. Khandekar, A. Meyerson, K. Munagala, and V. Pandit, “Local search heuristic for k-median and facility location problems,” in *Proceedings of the thirty-third annual ACM symposium on Theory of computing*, pp. 21–29, ACM, 2001.
- [23] “The MOSEK optimization software.”
- [24] M. A. Fischler and R. C. Bolles, “Random sample consensus: A paradigm for model fitting with applications to image analysis and automated cartography,” *CACM*, 1981.
- [25] C. Rao, *Operations Research*, vol. 1. Alpha Science International, 2005.
- [26] A. Schrijver, *Theory of Linear and Integer Programming*, vol. 1. Alpha Science International, 2005.
- [27] I. Heller and C. Tompkins, “An extension of a theorem of dantzig’s,” in *Linear Inequalities and Related Systems*, vol. 38, pp. 247–254, Princeton University Press, 1956.